J. Phys. Chem. A **2009,** *113,* 11833–11844

Metal−Phosphine Bond Strengths of the Transition Metals: A Challenge for DFT†

Yury Minenkov, Giovanni Occhipinti, and Vidar R. Jensen*

Department of Chemistry, University of Bergen, Allégaten 41, N-5007 Bergen, Norway

Received: March 31, 2009; Revised Manuscript Received: August 10, 2009

Previous promising tests of the new M06 family of functionals in predicting ruthenium−metal phosphine bond dissociation energies (Zhao, Y.; Truhlar, D. G. *Acc. Chem. Res.* **2008**, *41*, 157) have been extended to a series of phosphine complexes of chromium, molybdenum, nickel, and ruthenium for which relevant experimental data are available. In addition to the M06 family of functionals, bond dissociation enthalpies have been calculated using a selection of density functionals and hybrid functionals based on the generalized gradient approximation (GGA), and with or without an empirical term (i.e., DFT-D) accounting for long-range dispersion. For the ruthenium complexes, second-order Møller−Plesset perturbation theory (MP2) has also been applied. Electrostatic and nonelectrostatic solvent effects have been estimated using the polarizable continuum model (PCM), allowing for comparison with experimental data obtained for dissociation reactions in organic solvents. Whereas the GGA and hybrid-GGA functionals grossly underestimate the absolute metal−phosphine bond enthalpies, with mean unsigned errors (MUEs) for a set of 10 phosphine dissociation reactions in the range 13−27 kcal/mol, the recently developed DFT-based methods for inclusion of attractive noncovalent interactions and dispersion (the DFT-D and M06 functionals) dramatically improve upon the situation. The best agreement with experiment is observed for BLYP-D (MUE = 2.2 kcal/mol), and with the exception for M06-2X, all these methods provide MUEs well below 5 kcal/mol, which should be sufficient for a broad range of applications. The improvements in predicted relative bond enthalpies are less convincing, however. In several cases the GGA and hybrid-GGA functionals are better at reproducing substitution effects than the DFT-D and M06 methods.

Introduction

Density functional theory (DFT)[1] is the workhorse of contemporary applied quantum chemistry[2] and is routinely used in the study of realistic chemical systems. Even though such systems often involve a large number of atoms, the underlying generalized gradient approximation (GGA) does not account for noncovalent dispersion-type interactions,[3] leading to significant and systematic errors, in, e.g., calculated heats of formation of organic molecules when using popular functionals such as the hybrid-GGA B3LYP which incorporates some Hartree−Fock (HF) exchange.[4,5] Similarly, transition-metal (TM) chemistry has been a very active field of application for DFT[6] but has proven to pose particular problems, in particular for hybrid functionals, with large errors recorded in a number of validation and benchmark studies.[7,8] And of course, with the added problem of dispersion-type interactions, the accuracy of DFT in TM chemistry must be expected to be particularly questionable for large systems, affecting the description not only of intermolecular interactions but also of the treatment of intramolecular interactions such as those occurring between bulky ligands in a coordination compound.[7]

Recent years have seen a lot of effort to ameliorate the above-mentioned (and other) shortcomings of DFT. For example, Grimme has proposed an empirical term for long-range dispersion,[9] and inclusion thereof (termed DFT-D) improves upon the prediction of molecular structure and bond energies of noncovalently bound complexes,[4,10,11] intermolecular interaction energies in DNA bases pairs and amino acid pairs,[9] and reaction energies in organometallic chemistry.[10]

Nonlocal correlation effects may also be included using wave function methods based on the Kohn−Sham (KS) self-consistent field (SCF) solution, as for example in the double-hybrid density functionals (DHDF)[12,13] where a perturbative second-order correction has been shown to include in particular midrange correlation effects. By including also long-range effects through the above-mentioned empirical correction, the resulting methods (e.g., B2PLYP-D and mPW2PLYP-D) show excellent performance in a range of tests where standard DFT fails.[13,14] The superior performance, however, comes at the expense of slow basis-set convergence and a second-order term which scales with the fifth power of the number of basis functions. It thus seems unlikely that DHDF-based methods will replace SCF-only DFT in the large-system application segment.

In contrast, the latest "Minnesota family" of functional (termed M06) developed by Zhao and Truhlar[15,16] seems very promising for application to larger systems. These functionals have been constructed to account for effects of noncovalent interactions and include variable amounts of HF exchange, from zero in the local M06-L functional to full HF exchange in the M06-HF hybrid functional. Each individual functional has been designed for a particular application area and, taken together, the M06 class shows very good "across the board" performance and in particular improves upon standard functionals such as B3LYP in cases where noncovalent interactions are important.[17]

Several comparative studies indicate that the above-mentioned DFT-based methods, DFT-D, DHDF-D, and the M06 functionals, seem to group together in tests and thus to distinguish themselves from standard functionals not designed to account for noncovalent interactions. For example, van Mourik[18] has

---

† Part of the "Walter Thiel Festschrift".

* To whom correspondence should be addressed. E-mail: Vidar.Jensen@kj.uib.no. Telephone: (+47) 555 83489. Fax: (+47) 555 89490.

10.1021/jp902940c CCC: $40.75

SCHEME 1: Phosphine Dissociation in Gas Phase (GP) and in Toluene (Tol) for Ruthenium−Benzylidene Complexes ($L(PCy_3)X_2Ru{=}CHPh$)

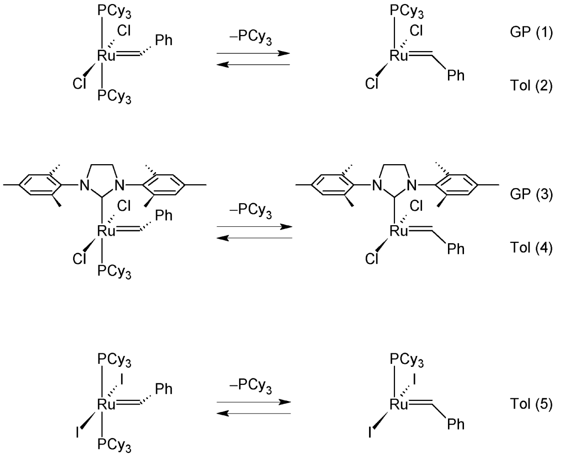

shown that, in contrast to B3LYP and X3LYP, the M06 functionals, DHDF and DHDF-D functionals, and DFT-D are able to locate all three minima along the coordinate of relative Tyr-Gly rotation. Peverati and Baldridge[19] have demonstrated good performance of M06-2X, BMK, and B97-D in studies of large polynuclear aromatic systems and molecules on metal surfaces. Good overall performance is also noted for B2PLYP (a DHDF method), but at considerably higher computational cost.

Returning now to transition-metal chemistry, metal−ligand bond dissociation energies of dative (noncovalent) ligands represent one case where standard DFT often is at odds with experiment. A telling example is offered by the relative ruthenium−phosphine bond enthalpies in various ruthenium complexes, $L(PCy_3)Cl_2Ru{=}CHPh$ (where L is a phosphine or N-heterocyclic carbene (NHC) ligand) for olefin metathesis; see Scheme 1.[20] As has been thoroughly documented by Tsipis et al.,[21] standard DFT predicts, incorrectly, that the ruthenium−tricyclohexyl phosphine bond enthalpy of the so-called second-generation catalyst (L = 1,3-dimesityl-4,5-dihydro-2-ylidene) is lower than that of the first-generation catalyst (L = tricyclohexyl phosphine). Recently, Zhao and Truhlar showed that their new M06 family of functionals in general, and M06-L in particular, is able to reproduce the difference between the two bond enthalpies to within experimental accuracy,[15,22] and they ascribe their success to the inclusion of medium range correlation effects and attractive noncovalent interactions (dispersion) that are not accounted for in the standard functionals.

The latter promising results on phosphine dissociation prompts the question of whether other recently developed DFT-based methods for the treatment of noncovalent interactions (vide supra) would also be able to capture the difference between the two reactions in Scheme 1. Of particular interest in this respect is to what extent a simple empirical term for long-range dispersion (DFT-D) improves upon the standard DFT results. In the event that the resulting DFT-D functionals would group together with M06-L for this difficult test case, it could be argued that the effects controlling the difference in dissociation rate between the first- and second-generation catalysts are predominantly long range. And of course, decent performance of a computationally inexpensive dispersion term in combination with a range of functionals available in popular electronic structure codes would be interesting from the point of view of future application to large, realistic organometallic systems.

Next, the accurate relative bond enthalpies reported by Zhao and Truhlar[22] raise the question of to what extent it is possible to obtain also absolute bond enthalpies that are comparable to those obtained in solution experiments. Such a quantitative comparison was not included, but the authors noted that “An accurate treatment of solvent effects must account for the competition between cavitation, dispersion, and electrostatic effects and would be an interesting subject for future study.”[22] Improvements to calculated bond enthalpies not only are important for obtaining accurate bond parameters but would have important implications in a number of areas. For example, phosphine dissociation and association reactions constitute key elementary steps in a number of catalytic reactions such as hydrogenation[23] and olefin metathesis[24] (Scheme 1), and a better description of the energetics of these steps will carry over in more accurate calculated activation parameters.

Finally, the role of dative ligands in coordination chemistry in general, and phosphines in particular, means that the advancements reported by Zhao and Truhlar[22] are of great importance if they extend to a broad range of phosphine dissociation reactions, or even to dissociation reactions of other dative ligands.

In order to investigate the above prospects of applying the recently developed cost-efficient methods for incorporation of noncovalent interactions in DFT, we have identified several complexes for which phosphine bond enthalpies can be inferred from experimental data. These include both early and late transition metals (Cr, Ni, Mo, and Ru) from the first and second row, several phosphine ligands, and a few organic solvents. In total, this results in a diverse validation set consisting of 10 individual dissociation reactions.

To the above test set, we have applied a range of standard GGA functionals (BLYP, PBE, BP86), hybrid-GGA functionals (B3LYP, B98), as well as a recently developed meta-GGA functional (M06-L) and hybrid counterparts thereof (M06, M06-2X, M06-HF). In addition, for BLYP, PBE, BP86, and B3LYP, we have added the dispersion term proposed by Grimme[9] to include also the resulting DFT-D functionals in the comparison.

Most of the available experimental bond enthalpies have been obtained for reactions in organic solvents. To allow for comparison with the experimental values, solvent effects as obtained using scaled particle theory (SPT)[25] and the polarizable continuum model (PCM)[26,27] have been included in the calculated bond enthalpies. Keen attention has been paid to conformational issues, and conformational searches have been performed at the force-field level prior to the local-minima geometry optimizations using DFT.

2. Computational Details

2.1. Conformational Issues. The organometallic compounds of the present work all possess a large number of possible conformations. For the ruthenium-based complexes, the conformations were taken from the detailed investigation of Tsipis et al.[21] For the other compounds, the most stable conformations were identified using the following procedure. For each compound, a starting geometry (conformation) was generated by performing a local-minimum geometry optimization and Hessian matrix calculation using DFT (vide infra). Next, conformational searches were performed at the MM3 force field level[28] using the SCAN program of the Tinker 4.2 molecular modeling software package.[29] All metal−ligand bond distances were kept at their original DFT-optimized values during the conformational searches. In some cases, selected angles and dihedral angles also had to be frozen in order to preserve the principal and already known coordination geometry of the metal atom (e.g., square planar) in the force-field-based geometry optimizations. Parameters necessary for energy evaluation of the metal complexes, but that were missing in the standard MM3 force field, were obtained from the harmonic force field of the initial DFT calculation (vide supra) using the SHRINK program.[30] A few unknown force constants of dihedral angles involving the central metal atom were set to zero.

2.2. Optimizations of Local Minima. The lowest-energy geometries obtained from the force-field-based conformational search were used as input structures in the geometry optimizations. The latter were performed using the three-parameter hybrid functional of Becke (termed B3LYP)[31] as implemented in the Gaussian 03 suite of programs.[32] Numerical integrations were performed using the default fine grid of Gaussian 03, and the Gaussian 03 default values were adopted for the self-consistent-field (SCF) and geometry optimization convergence criteria. The SCF solutions were routinely tested for instabilities,[33] both prior to and subsequent to geometry optimization. Stationary geometries were characterized by the eigenvalues of the analytically calculated Hessian matrix. Translational, rotational, and vibrational partition functions for thermal corrections to give total enthalpies were computed within the ideal-gas, rigid-rotor, and harmonic oscillator approximations following standard procedures. The temperatures used in the calculation of thermochemical corrections were identical to, or close to, those used in the corresponding experimental studies: 388.0 K for *trans*-$Cr(CO)_4(P(n\text{-}Bu)_3)_2$, 328.0 K for *trans*-$Cr(CO)_4(PPh_3)_2$, 325.0 K for *cis*-$Mo(CO)_4(PPh_3)_2$, and 298.15 K for all dissociation processes of Ni- and Ru-based complexes.

Effective core potentials (ECPs) of the Stuttgart type were used for all non-hydrogen elements, thereby reducing both the computational cost and the basis set superposition error (BSSE, vide infra). The ECPs accounted for the inner electrons of C (two-electron ECP), N (2), O (2), P (10), Cl (10), and I (46), and were used in combination with their corresponding [2s2p] (C, N, P) and [2s3p] (O, Cl, I) contracted valence basis sets.[34] Single sets of polarization d functions, obtained from the EMSL basis set exchange Web site,[35] were added to the basis sets of P (exponent $\alpha_d = 0.465$), Cl ($\alpha_d = 0.619$), and I ($\alpha_d = 0.266$). Similarly, ECPs were applied for Cr (10-electron ECP), Ni (10), Mo (28), and Ru (28), and accompanied by (8s7p6d)/[6s5p3d] contracted valence basis sets.[36] Hydrogen atoms were described by a Dunning double-ζ basis set.[37]

2.3. Single-Point Energy Evaluations. The energy was reevaluated at the optimized geometry, using the GGA functionals BLYP,[38,39] PBE,[40] and BP86,[38,41] the hybrid-GGA functionals B3LYP[31] and B98,[42] as implemented in the Gaussian 03 suite of programs.[32] Single-point (SP) evaluations using the recently developed meta-GGA functional (M06-L) and hybrid counterparts thereof (M06, M06-2X, M06-HF[40])[15] were performed using NWChem 5.1.[43]

Whereas the ECPs described above were retained in the single-point (SP) evaluations, the valence basis sets were improved compared to those used in the geometry optimizations. For the transition metals, two f functions[44] were added to the (8s7p6d) primitive basis sets.[36] The resulting (8s7p6d2f) primitive basis sets were contracted to [7s6p4d2f]. The valence basis sets of all nonmetal and non-hydrogen elements described above[34] have been supplemented by single sets of diffuse s and p functions obtained even-temperedly and, for those elements for which such functions were not part of the geometry optimization basis set, also by polarization d functions (C, $\alpha_d = 0.72$; N, $\alpha_d = 0.98$; O, $\alpha_d = 1.28$). The resulting (5s5p1d) (C, N, P) and (5s6p1d) (O, Cl, I) primitive basis sets were contracted to [4s4p1d] (C, N, P) and [4s5p1d] (O, Cl, I). Hydrogen atoms were described by a Dunning triple-ζ basis set[37] augmented by a diffuse s function ($\alpha_s = 0.043152$), obtained even-temperedly, and a polarization p function ($\alpha_p = 1.00$).

The above-described approaches to geometry optimization and SP calculations have been based on the use of ECPs, mainly for reasons of computational efficiency. Supplementary calculations on $(PCy_3)_2Cl_2Ru{=}CHPh$ have been performed to test the effects of using the above-mentioned ECPs compared to all-electron basis sets of similar quality. For example, with all carbon atoms described by all-electron [3s2p] contracted Dunning-Hay basis sets[37] (geometry optimization) or such basis sets extended to [5s4p1d] (SP calculation, extended as described above for the ECP basis sets) the resulting CPU time needed for completing an SCF procedure (B3LYP) was found to increase by 16% and 35% in the geometry optimization and SP calculation, respectively.

For dissociation reactions 2−4 (Scheme 1), SP calculations using Møller−Plesset second-order perturbation theory (MP2)[45] were also performed. Counterpoise corrections[46] were calculated and subtracted to remove basis set superposition errors. The basis sets used in the MP2 calculations were modified and extended compared to those described above for the DFT SP calculations. For phosphorus, the single d polarization function was replaced by two primitive d and one primitive f functions ($\zeta_d = 0.216$ and 0.652, $\zeta_f = 0.452$).[47] The basis set of the carbon atom of the N-heterocyclic carbene trans to the dissociating phosphine in reactions 3 and 4 (Scheme 1) was extended in an analogous fashion ($\zeta_d = 1.097$ and 0.318, $\zeta_f = 0.761$),[48] and the two thus modified primitive valence basis sets were contracted to [4s4p2d1f]. Finally, the ruthenium SP basis set described above was completed by addition of a single polarization *g* function ($\zeta_g = 1.057$).[44]

For the energy evaluations using the BLYP, PBE, BP86, and B3LYP functionals, we have added the dispersion term proposed by Grimme[9] to arrive at the resulting DFT-D estimates,

$$E_{\text{DFT-D}} = E_{\text{KS-DFT}} + E_{\text{disp}} \tag{1}$$

Here, $E_{\text{KS-DFT}}$ is the Kohn−Sham SCF energy and E_{disp} is the empirical dispersion correction, which, according to Grimme,[9] may be obtained as

$$E_{\text{disp}} = -s_6 \sum_{i=1}^{N_{\text{at}}-1} \sum_{j=i+1}^{N_{\text{at}}} \frac{C_6^{\,ij}}{R_{ij}^{\,6}} f_{\text{dmp}}(R_{ij}) \tag{2}$$

where N_{at} is the number of atoms, $C_6^{ij}$is the dispersion coefficient for atom pair *ij* with interatomic distance R_{ij}. The global scaling factor s_6 is only dependent on the density functional used, the values of which have been determined by Grimme (s_6(B3LYP, BP86) = 1.05, s_6(BLYP) = 1.20, s_6(PBE) = 0.75).[10] The damping factor f_{dmp} needed to avoid near-singularities and double-counting of correlation effects for small R_{ij} is given by

$$f_{\text{dmp}}(R_{ij}) = \frac{1}{1 + e^{-d(R_{ij}/R_r - 1)}} \tag{3}$$

Here, R_r is the sum of the atomic van der Waals radii[10] and *d* is a factor determined to 20.[10]

Electrostatic and nonelectrostatic solvent effects were estimated by the polarizable continuum model (PCM)[26,27,49] as implemented in Gaussian 03.[32] The solute cavity was constructed using the united atom topological model with atomic radii optimized for Hartree−Fock (termed “UAHF”) as recommended in the Gaussian 03 manual for the calculation of free energies of solvation; see also refs 26 and 50 as well as the useful discussions in refs 51 and 52. Moreover, additional calculations show very good agreement between net enthalpic solvent effects ($\Delta\Delta H_s$) obtained at the B3LYP and HF levels for reactions 2 and 4 (Scheme 1), with differences in the range 0.4−0.6 kcal/mol (see the Supporting Information for details).

Except for decane and tetrachloroethylene, for which parameters are not available in Gaussian 03, the internal program values for dielectric constants, number densities, etc., were adopted for the individual solvents used. For decane and tetrachloroethylene, the corresponding parameters for heptane and carbontetrachloride were used instead.

Common continuum solvation models such as PCM,[26,50] SMTs,[51,53] COSMO,[54] and Jaguar[55] are constructed to calculate Gibbs free energies of solvation and provide no direct information about other thermodynamics functions of solvation. In order to form reaction enthalpies (bond dissociation enthalpies), the enthalpic contribution to the free energy of solvation has been extracted as explained in the following procedure which is similar to that described earlier by Pais et al.[56] Additional tests as well as discussion of this procedure is given in the first part of the Results and Discussion section.

According to the scaled particle theory,[25] the molar heat of solution is given by

$$\Delta H_S = \bar{H}_c + \bar{H}_i \tag{4}$$

where $\bar{H}_c$ is the partial molar enthalpy needed to create a cavity for the solute in the solvent, $\bar{H}_i$ is the partial molar enthalpy of interaction of a solute molecule with a solvent in accordance with some potential law, and we assume the same concentration of a solute in the gas and liquid phases. Next, the entropy change associated with the charging of the cavity is assumed to be zero, i.e., $\bar{S}_i = 0$, as discussed originally by Pierotti[25] and confirmed in subsequent works; see refs 56 and 57 and references therein. In other words, the partial molar free energy of interaction is assumed to be equal to the corresponding enthalpy of interaction, $\bar{G}_i = \bar{H}_i$. The enthalpy of interaction has thus been obtained as a sum of all the terms pertaining to free energy of interaction, i.e., all the electrostatic contributions to the free energy of solvation as well as the solute−solvent dispersion and repulsion energies as calculated using the standard PCM model implemented in Gaussian 03.[32] The B3LYP functional has been applied in these PCM calculations and the thus obtained solvent corrections were adopted for all other methods. Tests involving a range of different GGA and hybrid-GGA functionals showed that the variation in the bond dissociation enthalpy due to the functional used in the PCM calculation is on the order of ±0.1 kcal/mol for the Ru complexes of reactions 2 and 4.

The partial molar free energy associated with the cavity formation, $\bar{G}_c$, consists of both entropic ($\bar{S}_c$) and enthalpic ($\bar{H}_c$) contributions. For a hard-sphere solute i, with diameter σ_2, the latter enthalpy can be expressed as[25]

$$\bar{H}_{ci} = y\alpha_p RT^2(1-y)^{-3}[(1-y)^2 + 3(1-y)\mathcal{R} + 3(1+2y)\mathcal{R}^2] + y(RP/\rho k)\mathcal{R}^3 \tag{5}$$

where $y = \pi\rho\sigma_1^3/6$ and $\mathcal{R} = \sigma_2/\sigma_1$, α_p is the thermal expansion coefficient of the solvent, R is the gas constant, T is the absolute temperature, P is the pressure, k is the Boltzmann constant, ρ is the number density, and σ_1 is the hard-sphere diameter of the solvent. By analogy to an approach used for the free energy of cavitation,[58] the partial molar enthalpy of cavitation for the present molecules has been obtained as a sum of the contributions from the above individual hard spheres, i, as

$$\bar{H}_c = \sum_i^{\text{spheres}} \frac{A_i}{4\pi R_i^2}\bar{H}_{ci} \tag{6}$$

Here, A_i is the exposed van der Waals surface of sphere i as obtained using the unscaled atomic UAHF radii (vide supra). Finally, the temperatures used in the calculation of the cavitation enthalpies were identical to, or close to, those used in the corresponding experimental studies: 388.0 K for *trans*-$Cr(CO)_4(P(n\text{-}Bu)_3)_2$, 328.0 K for *trans*-$Cr(CO)_4(PPh_3)_2$, 325.0 K for *cis*-$Mo(CO)_4(PPh_3)_2$, and 298.15 K for all dissociation processes of Ni- and Ru-based complexes.

3. Results and Discussion

3.1. Enthalpies of Solvation. In the following we present tests and additional discussion of the procedure chosen for extraction of the enthalpic contributions to the calculated free energies of solvation. Regarding the motivation for such a separation, it should be noted that, despite the fact that common continuum solvation models are aimed at reproducing free energies of solvation, experimental enthalpies of solvation are in most cases more readily available. Enthalpies of solvation can be not only determined from direct experiments but also may be straightforwardly calculated from experimental enthalpies of solution, enthalpies of sublimation (crystalline solutes), or enthalpies of vaporization (liquid solutes). Moreover, in some cases the entropic contributions are substantial, resulting in large errors if the free energy of solvation is used as an approximation to the corresponding enthalpy; see Table S5 in the Supporting Information. Thus, some attempts have been made to extract enthalpies of solvation from the corresponding calculated free energies, either completely[56] or limited to the electrostatic component,[59] calculated using PCM. In the following we use standard states with the same concentration of the solute (1 mol/L) in both the gas and liquid phase. In cases where different standard states were originally used in the presentation of the experimental values, the thermodynamic functions have been recalculated to allow for comparison with the present results.

It has been suggested[56] that the interaction entropy is small and can be neglected. Calculations to estimate the interaction entropies based on the response of the electrostatic part of the Gibbs free energy upon small changes in the permittivity of the solvent, ε, and on the cavity size have been performed.[59] As expected,[25] the interaction entropies are small and negative (−0.33 e.u. for CH_4 in benzene, 0.0 e.u. for propylamine in water, and CH_4 in methanol and in ethanol, −2.18 e.u. for CO_2 in cyclohexane, −0.27 e.u. for C_2H_6 in toluene, −0.31 e.u. for CH_4 in carbon tetrachloride, −0.32 e.u. for CH_4 in chlorobenzene, and for C_2H_6 in acetone), thus justifying the neglect thereof in the current calculations of enthalpies of solvation.

Figure 1 shows the MUEs for the thermodynamic solvation functions as calculated for 82 solute−solvent combinations compiled in Table S5 in the Supporting Information. The cavitation enthalpies and Gibbs free energies have been calculated using three different approaches. Here, PC symbolizes

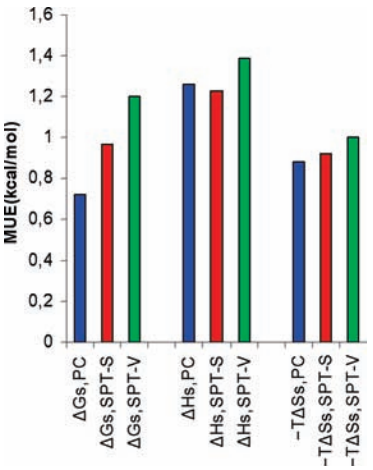

Figure 1. Mean unsigned error (MUE) for the Gibbs free energies, enthalpies and entropies of solvation for a total of 82 solute−solvent combinations listed in Table S5 in the Supporting Information. The effective solute cavity radius was calculated using the Pierotti−Claverie approach (PC), from the solute surface (SPT-S) or from the solute volume (SPT-V).

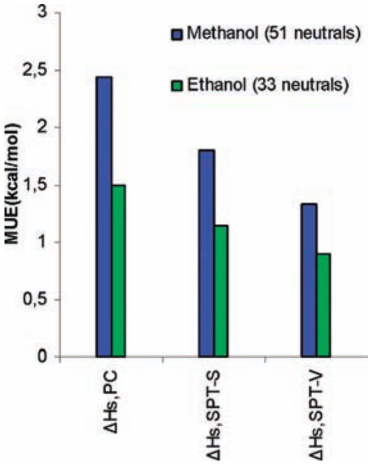

Figure 2. Mean unsigned error (MUE) for the enthalpies of solvation for a total of 51 solutes in methanol and 33 in ethanol, as compiled in Tables S6 and S7 in the Supporting Information. The effective solute cavity radius was calculated using the Pierotti−Claverie approach (PC), from the solute surface (SPT-S) or from the solute volume (SPT-V).

the Pierotti−Claverie approach described above, SPT-S stands for the scaled particle theory surface approach in which the radius of a solute cavity is calculated from the solute surface (originally, Pierotti[25] derived thermodynamic cavitation functions for spherical cavities), and SPT-V means the scaled particle theory volume approach in which the radius is calculated from the solute volume. The MUEs for the Gibbs free energy of solvation amount to 0.72, 0.97, and 1.2 kcal/mol for the PC, SPT-S, and SPT-V approaches to the cavity radius, respectively. These errors are somewhat smaller than those obtained by Cramer and Truhlar[53] for IEF-PCM, which is not surprising because our test set is smaller. Turning now to the enthalpies of solvation, the MUEs are somewhat higher, 1.26, 1.23, and 1.39 kcal/mol, respectively. This increase is expected because the PCM model has been trained to reproduce Gibbs free energies of solvation, not enthalpies, and also because we have neglected the interaction entropy as discussed above. The calculated solvation enthalpies are still accurate enough for the present work. Interestingly, the entropy of solvation can be reproduced with an accuracy higher than or comparable to that of the corresponding free energy.

Next, narrowing our focus to enthalpies of solvation only, experimental values are available for 51 neutral solutes in methanol and 33 neutral solutes in ethanol,[60] and these have been compiled in Tables S6 and S7 in the Supporting Information along with their calculated counterparts. The corresponding MUEs are presented in Figure 2. Again, the overall accuracy must be characterized as acceptable. Tomasi[50] noted that both SPT-S and SPT-V are better at reproducing solvation free energies than the Pierotti−Claverie approach, and this seems to be the case also for enthalpies. Despite the fact that SPT-S and SPT-V appear to offer higher accuracies for the calculation of solvation enthalpies, PC still is the method of choice in cases where “size consistency” is important, as discussed by Tomasi.[50] Size consistency is not relevant in studies limited to solvation of a single molecule but is of crucial importance for obtaining a smoothly changing cavitation energy along the reaction coordinate of dissociation or association processes. The Pierotti−Claverie approach has thus been applied in the present investigation of metal−ligand bond enthalpies.

3.2. Phosphine Dissociation in Ruthenium Complexes. Reactions 1−4 (Scheme 1) describe the initial loss of tricyclohexylphosphine from the 16-electron catalyst precursors of the first- and second-generation Grubbs’ catalysts for olefin metathesis.[61] These reactions have been thought to be barrierless,[21,62] an assumption that was supported by recent DFT calculations,[63] and their activation enthalpies[20,64] should therefore correspond closely to the ruthenium−phosphine bond energies. Despite the fact that the second-generation catalysts are known to be significantly more active than their first-generation counterparts, the initial phosphine dissociation is slower and, in fact, rate determining in the former.[20,64] This difference between the two catalysts, amounting to a 3.4 ± 2 and 3.5 kcal/mol higher bond enthalpy for the second-generation catalyst in solution[20,64] and gas-phase[63] experiments, respectively, is counterintuitive because one would expect a more pronounced trans influence[65] from the NHC than from the phosphine positioned trans to the leaving phosphine. Moreover, as shown by Tsipis et al.,[21] the difference turned out to be very difficult to reproduce by standard DFT methods, with the higher bond energies being obtained for the first-generation catalyst. Recently, Zhao and Truhlar[22] showed that their new M06-L functional is able to reproduce the difference between the two ruthenium−phosphine bond energies, and the absolute ruthenium−phosphine bond energies obtained in recent ESI-MS gas-phase experiments[63] closely match those predicted using the recently developed meta-GGA functional (M06-L).[22]

Initially avoiding the complications imposed by treatment of the solvent, we start by comparing the various calculated bond energies (including zero-point vibrational energies) with those of the ESI-MS gas-phase experiments;[63] see Figure 3. First, as was also seen for the accompanying BP86/ZORA calculations in the latter work,[63] the standard GGA and hybrid-GGA functionals (B3LYP, BP86, BLYP, PBE, and B98) dramatically underestimate the absolute binding energies, by more than 30 kcal/mol in the case of BLYP. In fact, Hartree−Fock groups together with the predictions of the standard functionals, whereas close to converged results are obtained even with a relatively simple wave function-based correlation treatment including correction (counterpoise method) for basis set superposition errors (MP2-CP). This illustrates that the failure of GGA and

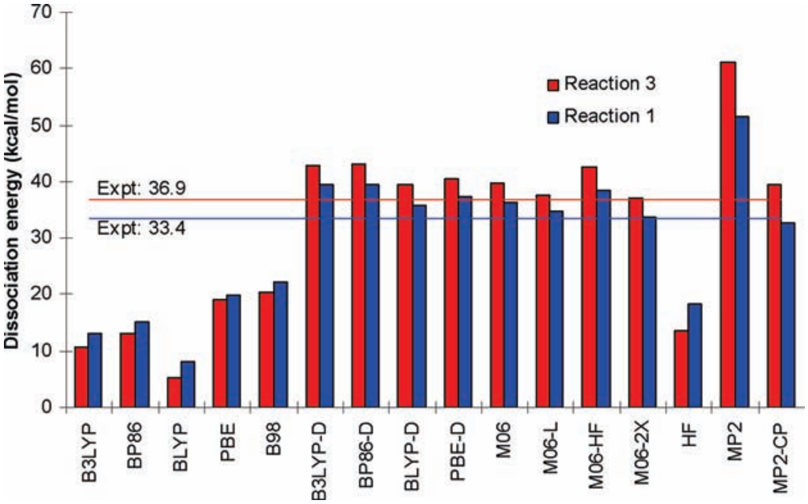

Figure 3. Phosphine bond dissociation energies at 0 K (i.e., including zero-point vibrational energies) for the first- and second-generation ruthenium-based Grubbs' catalysts as calculated and obtained in ESI-MS experiments, reactions 1 and 3 (Scheme 1).

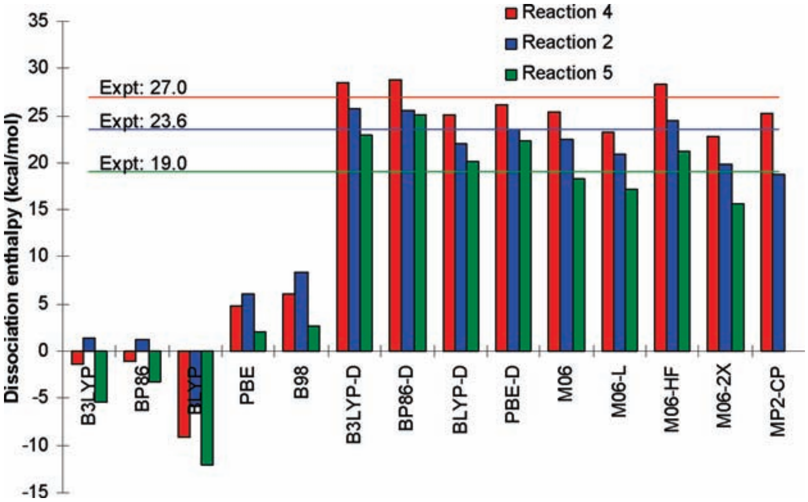

Figure 4. Phosphine bond dissociation enthalpies in toluene for the first- (reactions 2 and 5) and second-generation (reaction 4) ruthenium-based Grubbs' catalysts.

hybrid-GGA in reproducing the correct bond dissociation energy must originate from an incomplete treatment of electron correlation.

Next, also for the relative bond energies HF fails and predicts a higher bond energy for the first- than for the second-generation catalyst, exactly the problem noted previously for standard DFT.[21] And again, the qualitative problem disappears already at the MP2-CP level, although with a 3.5 kcal/mol overestimation of the difference between the bond energies of the first- and second-generation catalysts. Summing up, the uniform performance seen for HF and standard DFT in the absolute and relative bond energies for reactions 1 and 3, together with the fact that the shortcomings of HF may be corrected by a simple wave-function-based correlation treatment, strongly suggest that the success of the M06 class of functional in describing these energies is indeed due to the inclusion of "attractive noncovalent interactions".[15,22] Finally, that the latter interactions are at least not of short-range kind is confirmed by the fact that a dispersion term based on the correct long-range R^{-6}-behavior to a large extent is able to correct for the above problems. The resulting DFT-D absolute bond energies are overestimated by only a few kilocalories per mole and display an essentially correct relative magnitude for the first- and second-generation catalysts.

Comparing now the experimental absolute enthalpies for loss of phosphine in gas phase, reactions 1 and 3 (33.4 and 36.9 kcal/mol, respectively; Figure 3), with those obtained in toluene solution, reactions 2 and 4 (23.6 and 27 kcal/mol, respectively; Figure 4), it appears that the presence of the solvent together with the vibrational effects reduce the bond strength to ruthenium by a substantial amount (by almost 10 kcal/mol), an effect which is due in part to the dipole moment of the 14-electron complex being larger than that of the 16-electron adduct.[66] The bond dissociation energies in Figure 3 include zero-point vibrational effects and are lower than the corresponding gas-phase electronic values by 2.1 (reaction 1) and 2.3 kcal/mol (reaction 3), respectively. The additional effects of correcting to room temperature are miniscule and amount to an additional reduction (increase) of the bond enthalpy of 0.2 (0.1) kcal/mol for reaction 2 (reaction 4). Accordingly, it appears that almost all the difference between the gas-phase and solvent experimental enthalpies may be attributed to solvent effects. The calculated enthalpies for reaction 2 and 4 in Figure 4 have been corrected for electrostatic and nonelectrostatic solvent effects using PCM as described in Computational Details. The implicit solvent model is able to capture the (substantial) effects of adding solvent remarkably well and lower the bond enthalpy by 11.5 kcal/mol (reaction 2) and 12.1 kcal/mol (reaction 4), respectively. The solvent-induced lowering of the bond enthalpies is thus overestimated by 1−2 kcal/mol. This means that the methods that performed well for the gas-phase reactions

(Figure 3) are also in good agreement with the solution experiments after addition of the PCM corrections (Figure 4), although with a tendency toward underestimation of the absolute bond enthalpies. The inability of standard DFT methods in capturing important contributions to the ruthenium−phosphine bond is illustrated by the fact that several of the thus obtained bond dissociation enthalpies are negative after inclusion of solvent corrections.

In contrast to the above-mentioned significant solvent effects (∼10 kcal/mol) on the ruthenium−phosphine bond enthalpies determined experimentally and also calculated in the present work, Tsipis et al.[21] reported that their bond energies were "barely modified" by the solvent effects calculated using the self-consistent reaction field continuum model implemented in the Jaguar 4.0 program.[67] The latter model is similar to the integral equation formalism (IEF) PCM model used in the present work, and the results should therefore be comparable. Tsipis et al.[21] only included electrostatic contributions,[68] and their finding that such solvent effects have little influence on the bond energies is indeed corroborated by the fact that the presently calculated electrostatic part of the net enthalpic solvent effects ($\Delta\Delta H_s$) on reactions 2 and 4 is between −1 and −2 kcal/mol; see Tables S3 and S4 in the Supporting Information. The net enthalpic solvent effects are thus dominated by the nonelectrostatic contributions and in particular by the solute−solvent dispersion term.

The relative effect of the solvent corrections is to lower the bond enthalpy of the second-generation catalyst by 0.6 kcal/mol compared to the first-generation catalyst. Half of this difference is masked by the vibrational temperature corrections (vide supra) from 0 K, and the methods that performed well for the gas-phase reactions reproduce the relative bond enthalpies well also in solution.

Turning now to the effect of replacing chloride by iodide as ligand in the equatorial plane, with a relative enthalpy difference ($\Delta\Delta H$) amounting to −4.6 kcal/mol, compare reactions 2 and 5 in Figure 4; all the methods predict, correctly, that the iodide compound has a lower phosphine dissociation enthalpy. The methods differ substantially, however, in predicting the magnitude of this effect. In fact, the GGA and hybrid-GGA methods perform reasonably well and all predict a markedly lower bond enthalpy for the iodide compound, the substituent effect being overestimated in particular for BLYP and B3LYP. The empirical dispersion term more than corrects for this and appears to effectively overshoot the stability of the 16-electron iodide complex and cancels much of the difference in bond enthalpy predicted by the parent DFT methods. Finally, the M06 functionals perform well and fairly consistently and are superior to the standard DFT and DFT-D methods included here in reproducing this substitution effect.

3.3. Phosphine Dissociation in Molybdenum and Chromium Complexes. Metal−phosphine bond dissociation enthalpies have been derived from kinetic measurements of CO replacement studies on *cis*-Mo(CO)$_4$(PPh$_3$)$_2$,[69] *trans*-Cr(CO)$_4$(P(*n*-Bu)$_3$)$_2$,[70] and *trans*-Cr(CO)$_4$(PPh$_3$)$_2$.[71] These replacement reactions can be written as reaction 6,

$$\mathrm{M(CO)_4L_2 + CO \rightarrow M(CO)_5L + L} \tag{6}$$

where M is Cr or Mo and known to follow rate laws that are first order with respect to the bis(phosphine) complexes. The initial dissociation of phosphine is thus rate determining; see Scheme 2. Moreover, the transition states (TSs) of dissociation have been found to resemble closely the products of dissociation, and the activation enthalpies are expected to represent useful approximations to the bond dissociation enthalpies.[69,71]

SCHEME 2: Phosphine Dissociation in Tetrachloroethylene (TCE) for *cis*-Mo(CO)$_4$(PPh$_3$)$_2$

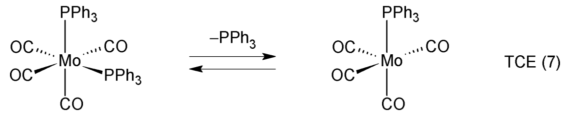

3.3.1. Dissociation in cis-Mo(CO)$_4$(PPh$_3$)$_2$. Geometry optimization followed by SP energy evaluations have been performed using both singlet and triplet spin multiplicity for *cis*-Mo(CO)$_4$(PPh$_3$)$_2$ and the 16-electron dissociation product. All methods of the present work predict the singlet state of both the 18- and 16-electron complexes to be the most stable by a good margin, e.g., by 39.8 and 24.8 kcal/mol for the 18- and 16-electron complex, respectively, using B3LYP. The optimized geometry of singlet *cis*-Mo(CO)$_4$(PPh$_3$)$_2$ reveals an essentially octahedral coordination around the manganese atom, although with some distortions due to the cis-positioned triphenylphosphine groups (Figure 5). These structural features are to a large extent preserved during dissociation, the 16-electron dissociation product displaying, as expected, an essentially tetragonal pyramidal geometry.

The experimental and calculated bond dissociation enthalpies for *cis*-Mo(CO)$_4$(PPh$_3$)$_2$ in tetrachloroethylene solution (reaction 7, Scheme 2) are depicted in Figure 6. As noted above for dissociation in the ruthenium complexes, standard DFT grossly underestimates the experimental value, by more than 25 kcal/mol in the worst case (BLYP). And again, the addition of a long-range empirical dispersion term dramatically improves the agreement with experiment. BLYP-D practically reproduces experiment, whereas for the other functionals, a tendency toward overcorrection from the dispersion term may be noticed. With the exception of M06-HF, which, similarly to B3LYP-D, BP86-D, and PBE-D, overshoots by a few kilocalories per mole (up to almost 5.1 kcal/mol for BP86-D), the M06 functionals perform excellently in predicting this dissociation enthalpy.

3.3.2. Dissociation in trans-Cr(CO)$_4$(P(n-Bu)$_3$)$_2$ and trans-Cr(CO)$_4$(PPh$_3$)$_2$. For *trans*-Cr(CO)$_4$(P(*n*-Bu)$_3$)$_2$ and *trans*-Cr(CO)$_4$(PPh$_3$)$_2$, geometry optimization followed by SP energy evaluations have been performed using both singlet and triplet spin multiplicity. As for the molybdenum complexes above, a range of different methods predict the singlet state to be the most stable, by 44.8 and 24.1 kcal/mol for *trans*-Cr(CO)$_4$(P(*n*-Bu)$_3$)$_2$ and *trans*-Cr(CO)$_4$(PPh$_3$)$_2$, respectively, using B3LYP, the optimized geometries of which are shown in Figure 7. Due

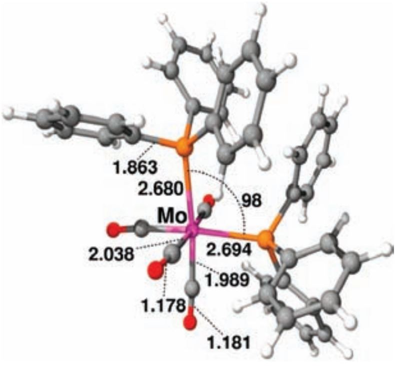

Figure 5. DFT-optimized geometry of *cis*-Mo(CO)$_4$(PPh$_3$)$_2$. Selected bond distances are given in angstroms and bond angles in degrees. Color coding: C, gray; H, white; O, red; P, orange; Mo, pink.

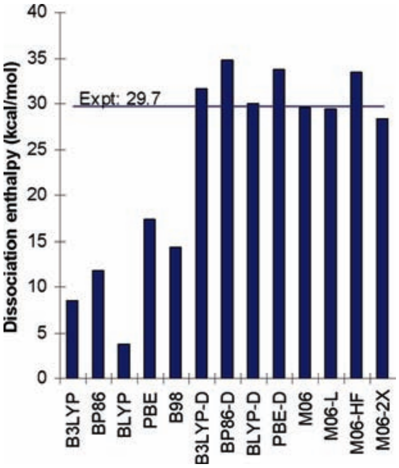

Figure 6. Phosphine bond dissociation enthalpies for *cis*-$Mo(CO)_4(PPh_3)_2$ in tetrachloroethylene (reaction 7).

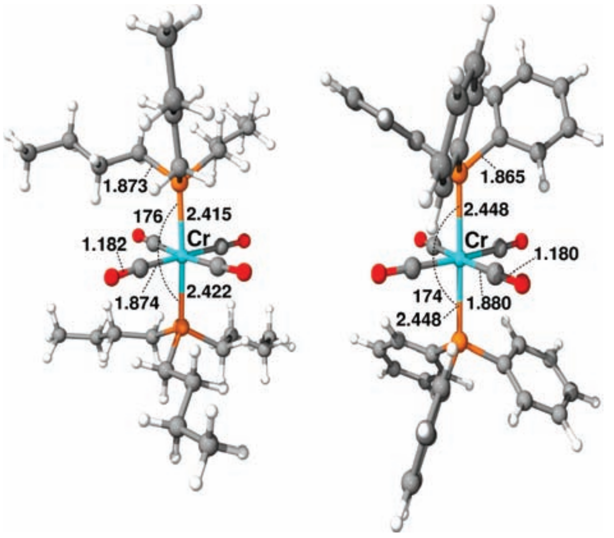

Figure 7. DFT-optimized geometries of *trans*-$Cr(CO)_4(P(n\text{-}Bu)_3)_2$ (left) and *trans*-$Cr(CO)_4(PPh_3)_2$ (right). Selected bond distances are given in angstroms and bond angles in degrees. Color coding: C, gray; H, white; O, red; P, orange; Cr, turquoise.

to the increased distance between the bulky phosphine groups, the two 18-electron trans complexes deviate less from ideal octahedral geometry than the molybdenum cis complex (Figure 5).

As for the Mo complex, the activation parameters for *trans*-$Cr(CO)_4(P(n\text{-}Bu)_3)_2$ and *trans*-$Cr(CO)_4(PPh_3)_2$ indicate that the TS for dissociation involves a product-like geometry from which the phosphine has been completely disconnected.[70] In the TS, the remaining phosphine is expected to occupy an axial position of a square pyramid.[70,71] The corresponding geometry with the phosphine in an equatorial position is known to be of lower energy[72] and is probably located later on the potential energy surface of dissociation.[70,71] Consequently, we have only studied square-pyramidal complexes featuring the phosphine in axial position as models for the TS of dissociation; see Scheme 3. In geometry optimizations of spin triplet complexes of this kind, the phosphine quickly relaxes toward an equatorial position and this spin multiplicity was therefore excluded from further study. In the optimized geometry for the singlet state, the triplet is calculated to be higher by 14.1 and 12.6 kcal/mol for the *trans*-$Cr(CO)_4(P(n\text{-}Bu)_3)_2$ and *trans*-$Cr(CO)_4(PPh_3)_2$ complexes, respectively, using B3LYP.

SCHEME 3: Phosphine Dissociation for *trans*-$Cr(CO)_4(P(n\text{-}Bu)_3)_2$ and for *trans*-$Cr(CO)_4(PPh_3)_2$ in *n*-Decane (Dec) and 1,2-Dichloroethane (DCE), Respectively

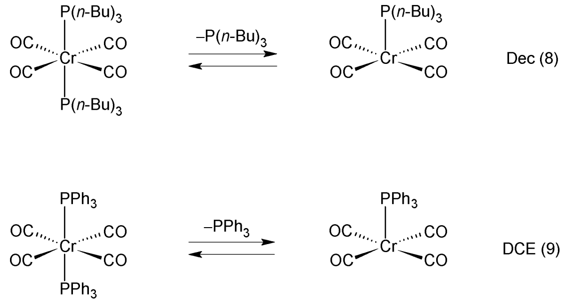

The enthalpies for reactions 8 and 9 (Scheme 3) are shown in Figure 8. The tendency of standard DFT to underestimate the metal−ligand bond strength of the dative phosphine ligand is clear also for these chromium complexes but is less pronounced than for the reactions above, in particular for the dissociation of triphenylphosphine (reaction 9). In fact, PBE is very close to getting the bond dissociation enthalpy for this reaction right, the prediction being too low by only 1.0 kcal/mol. Thus, not surprisingly, the addition of an empirical dispersion term results in significant overestimation for all the DFT-D methods, and by more than 10 kcal/mol for PBE-D and BP86-D. The DFT-D methods perform better for the dissociation of $P(n\text{-}Bu)_3$ (reaction 8), with predictions on both sides of the experimental value. All the M06 functionals underestimate the bond dissociation enthalpy of the latter reaction, although M06 by only 1.4 kcal/mol, whereas M06-L and M06 also overestimate the enthalpy of reaction 9, by 3.5 and 5.6 kcal/mol, respectively. Turning now to the difference between the two bond dissociation enthalpies, all the methods included in the present study underestimate the experimental $\Delta\Delta H$ (11.2 kcal/mol). In fact, the GGA and hybrid-GGA functionals are better at reproducing this $\Delta\Delta H$ than the methods including treatment of noncovalent interactions, with calculated enthalpy differences in the range 5.6−6.9 kcal/mol, compared to 3.1−3.8 and 2.9−4.2 kcal/mol for the DFT-D methods and the M06 family of functionals, respectively.

3.4. Phosphine Dissociation in Nickel Complexes. Bond dissociation enthalpies for loss of phosphine in $Ni(PEt_3)_3(CN)_2$

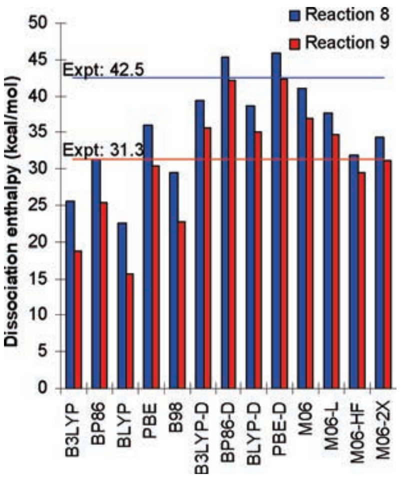

Figure 8. Phosphine bond dissociation enthalpies for *trans*-$Cr(CO)_4(P(n\text{-}Bu)_3)_2$ in decane (reaction 8) and *trans*-$Cr(CO)_4(PPh_3)_2$ in 1,2-dichloroethane (reaction 9) solution, respectively.

SCHEME 4: Phosphine Dissociation for $Ni(CN)_2(PEt_3)_3$ and $Ni(CN)_2(PEtPh_2)_3$ in Ethanol (EtOH) and 1,2-Dichloroethane (DCE)

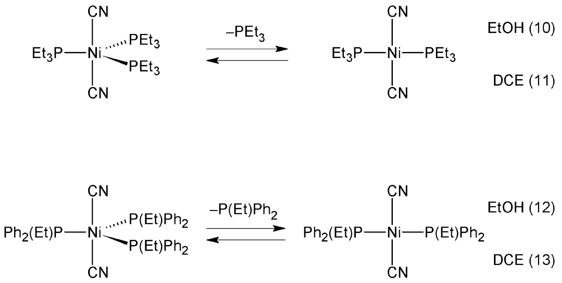

and $Ni(PEtPh_2)_3(CN)_2$ have been determined by measuring the equilibrium constants of reactions 10−13 (Scheme 4) spectrophotometrically at different temperatures.[73] All the Ni(II) compounds involved in these reactions are diamagnetic.[74] The geometries optimized for the five-coordinate complexes are, as expected, those of a trigonal bipyramid with all three phosphines in the equatorial plane (Figure 9), whereas in the planar, four-coordinate dissociation products, the phosphines are positioned trans to each other.

Figure 10 shows the calculated and experimentally determined bond dissociation enthalpies for $Ni(PEt_3)_3(CN)_2$ in ethanol (reaction 10) and dichloroethane (reaction 11) solutions. All GGA and hybrid-GGA functionals predict negative bond dissociation enthalpies, which again serves to underline the systematic underestimation of bond strength noted already for these methods. The methods designed to include effects from noncovalent interactions and dispersion perform significantly better than the standard functionals, with BP86-D and PBE-D essentially reproducing experiment. The other DFT-D methods and two of the functionals of the M06 family (M06 and M06-L) underestimate these enthalpies by a few kilocalories per mole (3.2−6.2 kcal/mol). The M06 functionals with the largest fractions of HF exchange (M06-2X and M06-HF) perform significantly worse and essentially predict reaction 10 to be thermoneutral. Finally, the difference due to change of solvent (2.7 kcal/mol) is seen to be remarkably well reproduced (2.5 kcal/mol) by the PCM approach.

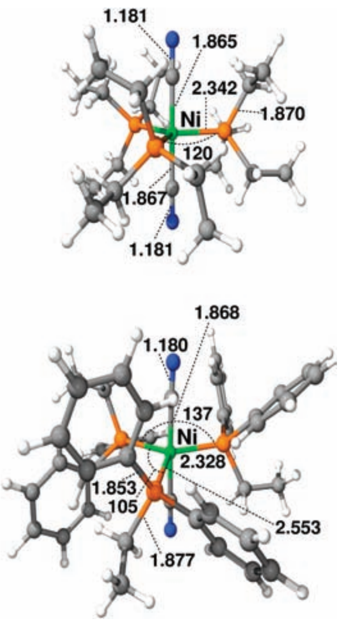

Figure 9. DFT-optimized geometries of $Ni(CN)_2(PEt_3)_3$ (upper) and $Ni(CN)_2(PEtPh_2)_3$ (lower). Selected bond distances are given in angstroms and bond angles in degrees. Color coding: C, gray; H, white; O, red; P, orange; N, blue; Ni, green.

Many of the comments given above for dissociation of triethylphosphine are true also for the dissociation of $PEtPh_2$ (reactions 12 and 13, Figure 10). However, for the latter dissociation, the methods accounting for noncovalent interactions and dispersion show fewer tendencies toward underestimation of the bond enthalpy than than seen above for triethylphosphine. With BP86-D and PBE-D now overshooting by up to 3.2−5.1 kcal/mol, near perfect agreement with experiment is provided by BLYP-D. Changing the solvent from ethanol to dichloroethane, i.e., going from reaction 12 to 13, results, according to experiment, in a 2.1 kcal/mol increase in the bond dissociation enthalpy, an effect which is 0.6 kcal/mol smaller than that seen for triethylphosphine above (reactions 10 and 11). Once again, PCM obtains the approximate magnitude of the solvent effects but fails, however, in reproducing the differential solvent effects. In fact, PCM predicts a small increase (from 2.5 to 2.8 kcal/mol) in the enthalpy difference between the two solvents upon going from PEt_3 to $PEtPh_2$.

The change in bond enthalpy resulting from changing the ligand can be derived from comparison of reactions 11 and 13 and 10 and 12, for which the experimentally derived relative enthalpy differences ($\Delta\Delta H$) is 4.5 and 3.9 kcal/mol, respectively. Whereas M06-HF and M06-2X do not even predict the correct relative order between the bond enthalpies for the two complexes, most of the DFT-D and the M06 methods predict qualitatively correct but too small relative enthalpy differences. In contrast, even if GGA and hybrid-GGA are far from able to reproduce the absolute enthalpies, they perform well for these relative enthalpy differences. B98, for example, gives 4.4 (reaction 11 vs 13) and 4.6 kcal/mol (10 vs 12) for the two relative enthalpy differences.

3.5. Overall Comparison and Concluding Remarks. As a means of comparing the different functionals and evaluating the accuracy of the estimates obtained after inclusion of the PCM solvent corrections, we provide the mean unsigned errors (MUEs) and mean signed errors (MSEs) for dissociation enthalpies calculated for the 10 dissociation reactions in organic solvents (reactions 2, 4, 5, and 7−13); see Figure 11.

The perfect negative relationship between the MUEs and MSEs for the GGA and hybrid-GGA functionals confirms the main issue noted above for the individual reactions: Standard DFT grossly underestimates the present bond dissociation enthalpies and must be regarded as unsuitable for applications, such as the prediction of reaction barriers involving phosphine dissociation or coordination, in which a fairly accurate description of the bond strength itself is expected to be important for a given calculated property. The extent of the problem is illustrated by the fact that in a number of cases (for reactions 2, 4, 5, 10, 11, 12, and 13) negative bond dissociation enthalpies are predicted by GGA or hybrid-GGA functionals, even when the corresponding experimental values are as high as 20−30 kcal/mol. Such discrepancies are of course conspicuous, and highlight the fact that standard DFT does not account for all the effects contributing to the strength of dative bonds. Problems similar to the ones described here for transition metal−phosphine bonds are likely to exist also for other dative ligands. Given the importance of metal−ligand dative bonds, the inability to properly describe them must be regarded as a serious drawback for the application of standard DFT to coordination chemistry and catalysis.

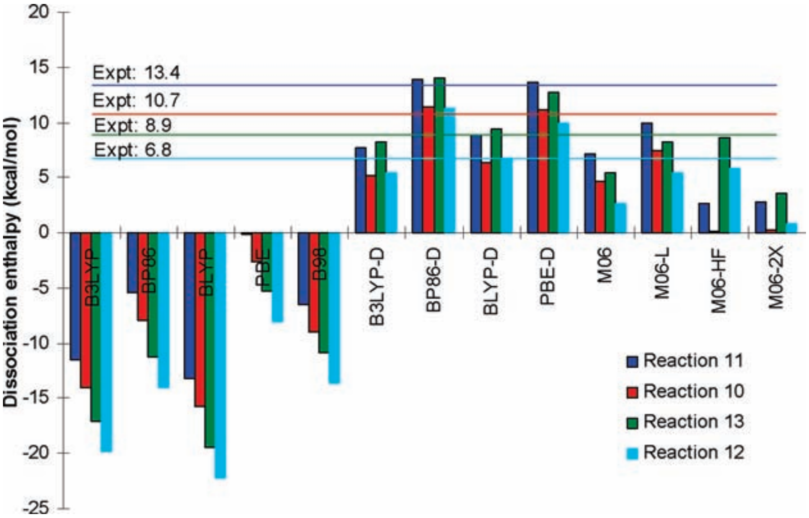

Figure 10. Phosphine bond dissociation enthalpies for $Ni(PEt_3)_3(CN)_2$ and $Ni(PEtPh_2)_3(CN)_2$ in ethanol (reactions 10 and 12) and 1,2-dichloroethane (reactions 11 and 13) solution, respectively.

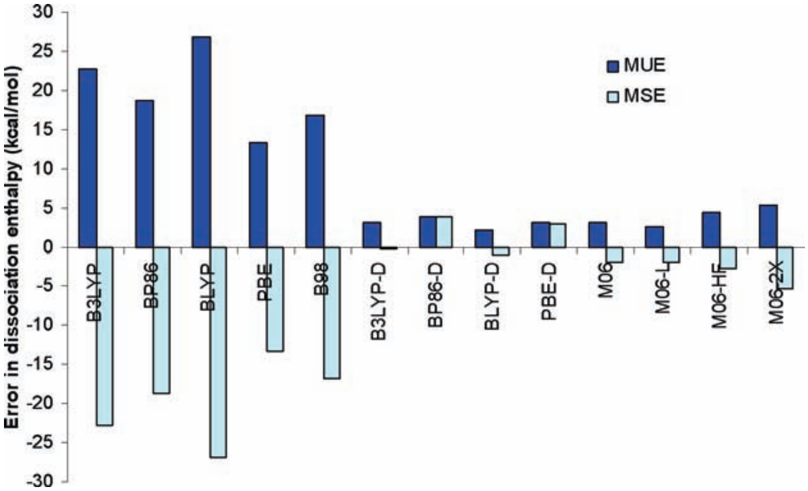

Figure 11. Mean unsigned error (MUE) and mean signed error (MSE) for the 10 metal−phosphine bond dissociation enthalpies (reactions 2, 4, 5, and 7−13) in organic solvents.

Fortunately, the efforts in recent years toward including treatment of attractive noncovalent interactions seem to be fruitful and to dramatically reduce the problems described above for standard DFT. The MUEs obtained for the DFT-D methods are in the range 2.2−3.9 kcal/mol, with a tendency toward overestimation for BP86-D and PBE-D. In fact, the best-performing method turns out to be BLYP-D, for which the parent BLYP functional actually provides the largest deviations from experiment among all the present methods. The MUE obtained for BLYP is even lower than those for M06-L and M06 (by 0.4 and 0.8 kcal/mol, respectively), and for which a MSE of only −1.1 kcal/mol bears witness of only insignificant systematic errors. The four functionals of the M06 family all tend toward underestimation of the bond enthalpies, with a clear negative MSE (−1.9 kcal/mol) for both M06-L and M06. As expected for reactions involving transition metals,[15] M06-L turns out to be the best performer in the M06 family, although with only a small margin, to the hybrid M06 functional. However, the results for M06-2X and M06-HF confirm that the errors increase upon inclusion of additional HF exchange and these functionals are also not recommended for application on transition-metal systems.[15]

It should be stressed, however, that the present data set is limited and that there is an added (although probably minor) uncertainty stemming from the fact that 6 of the 10 experimental bond dissociation enthalpies are actually activation enthalpies (vide supra). Too much significance should therefore not be assigned to a detailed ranking of the best functionals. In fact, the perhaps most encouraging conclusion that can be drawn from the present study is that, after addition of solvent effects, a range of contemporary methods for inclusion of attractive noncovalent interactions offers an overall accuracy (MUE) well below 5 kcal/mol. Although “chemical accuracy” is not achieved, the accuracy is still sufficient for application to a variety of questions and problems. More importantly, the accuracy is obtained at the computational cost of SCF DFT, with solvent effects accounted for in single-point calculations using an implicit solvent model. The overall approach is thus cost efficient and may be applied to relatively large systems.

On the negative side it should be noted that, in a couple of cases, the methods for treatment of noncovalent interactions and dispersion fail to reproduce relative enthalpy differences. Whereas the latter methods excel in reproducing the ruthenium−phosphine bond enthalpy difference between the first- and the second-generation Grubbs’ catalysts (e.g., reactions 2 and 4), they are less suited at predicting the change in bond enthalpy upon going from reaction 8 to 9 for the chromium complexes. Even worse, they fail in reproducing the relative enthalpy differences associated with changing the ligand in the nickel complexes (reactions 11 and 13 and 10 and 12), an effect essentially captured, at least qualitatively, by GGA and hybrid-GGA. DFT-D also significantly underestimates the effects of replacing chloride by iodide in the first-generation Grubbs' catalyst (reactions 2 and 5), and also in this case is the effect of substitution better handled by the parent DFT methods. In practice, it is often more important to reproduce differential rather than absolute thermochemical quantities. Thus, despite the convincing overall performance in reproducing absolute bond dissociation enthalpies seen for the new methods for incorporation of attractive noncovalent interactions, the above-mentioned inaccuracies in bond enthalpy differences are disappointing. The present results should, however, be complemented by other tests before general conclusions in this respect are drawn.

Finally, the gross underestimation of the bond strength of the metal−ligand dative bonds seen here prompts the question of how GGA and hybrid-GGA functionals have managed to defend their role as the main provider of useful, and, in many cases, surprisingly accurate, thermochemical parameters for transition-metal reactions, including bond enthalpies of metal−ligand dative bonds, over the last two decades. A possible clue as to the origin of this apparent puzzle has been noted already, e.g., by Harvey,[7] and is to be found in partial cancellation between effects from noncovalent interactions and solvation. Relative enthalpies and free energies obtained from gas-phase calculations only, i.e., without estimates of effects from solvent, have routinely been compared with values from experiments carried out in solution. The current results nicely illustrate the effects of error cancellation resulting from such practice. Whereas the PCM solvent corrections reduce the current bond enthalpies by an amount ranging from 3.5 (reaction 8) to 13.4 kcal/mol (reaction 12), the empirical dispersion correction contributes to increasing the bond enthalpies, by between 13.9 (reaction 7) and 29.9 kcal/mol (reaction 4), as obtained using B3LYP. The net effect of neglecting both these opposing contributions is substantial and fortuitous cancellation of errors. For example, the large MUE obtained for B3LYP (22.8 kcal/mol) is reduced by almost 10 kcal/mol if solvent effects are neglected. In fact, for the best-performing standard functional in the present work (PBE), the MUE falls below 5 kcal/mol if solvent corrections are excluded from the calculated enthalpies.

Acknowledgment. The Norwegian Research Council is acknowledged for financial support through the KOSK program (Grant No. 177322/V30) as well as for CPU resources granted through the NOTUR supercomputing program. University of Bergen is acknowledged for financial support through the Nanoscience program.

Supporting Information Available: Total energies, thermochemical corrections, dispersion corrections, solvent corrections, and Cartesian coordinates calculated for the individual compounds, as well as tabulated enthalpies represented in Figures 3, 4, 6, 8, and 10, tabulated mean signed and unsigned errors represented in Figure 11, and the individual solvation enthalpies forming the basis for Figures 1 and 2. This material is available free of charge via the Internet at http://pubs.acs.org.

Note Added after ASAP Publication. This article posted ASAP on September 8, 2009. In Section 2.3, a value has been revised in the first sentence following equation 3. The correct version posted on September 18, 2009.

References and Notes

(1) Hohenberg, P.; Kohn, W. *Phys. Rev.* **1964**, *136*, B864. Kohn, W.; Sham, L. J. *Phys. Rev.* **1965**, *140*, A1133.

(2) Chermette, H. *Coord. Chem. Rev.* **1998**, *178*, 699. Koch, W.; Holthausen, M. C. *A Chemist's Guide to Density Functional Theory*, 2nd ed.; Wiley-VCH: Weinheim, 2001. *Theory and Applications of Computational Chemistry: The First Forty Years*; Dykstra, C. E., Frending, G., Kim, K. S., Scuseria, G. E., Eds.; Elsevier: Amsterdam, 2005.

(3) Kristyan, S.; Pulay, P. *Chem. Phys. Lett.* **1994**, *229*, 175.

(4) Grimme, S. *J. Comput. Chem.* **2004**, *25*, 1463.

(5) Rokob, T. A.; Hamza, A.; Papai, I. *Org. Lett.* **2007**, *9*, 4279. Wodrich, M. D.; Corminboeuf, C.; Schleyer, P. V. *Org. Lett.* **2006**, *8*, 3631. (b) Wodrich, M. D.; Corminboeuf, C.; Schreiner, P. R.; Fokin, A. A.; Schleyer, P. V. *Org. Lett.* **2007**, *9*, 1851.

(6) Davidson, E. R. *Chem. Rev.* **2000**, *100*, 351.

(7) Harvey, J. N. *Annu. Rep. Prog. Chem., Sect. C, Phys. Chem.* **2006**, *102*, 203.

(8) Zhao, Y.; Truhlar, D. G. *J. Chem. Phys.* **2006**, *124*, n/a. Schultz, N. E.; Zhao, Y.; Truhlar, D. G. *J. Phys. Chem. A* **2005**, *109*, 11127. Furche, F.; Perdew, J. P. *J. Chem. Phys.* **2006**, *124*, 044103. Kameno, Y.; Ikeda, A.; Nakao, Y.; Sato, H.; Sakaki, S. *J. Phys. Chem. A* **2005**, *109*, 8055.

(9) Antony, J.; Grimme, S. *Phys. Chem. Chem. Phys.* **2006**, *8*, 5287.

(10) Grimme, S. *J. Comput. Chem.* **2006**, *27*, 1787.

(11) Jurecka, P.; Cerny, J.; Hobza, P.; Salahub, D. R. *J. Comput. Chem.* **2007**, *28*, 555. Pavone, M.; Rega, N.; Barone, V. *Chem. Phys. Lett.* **2008**, *452*, 333.

(12) Benighaus, T.; DiStasio, R. A.; Lochan, R. C.; Chai, J. D.; Head-Gordon, M. *J. Phys. Chem. A* **2008**, *112*, 2702.

(13) Schwabe, T.; Grimme, S. *Phys. Chem. Chem. Phys.* **2006**, *8*, 4398.

(14) Schwabe, T.; Grimme, S. *Acc. Chem. Res.* **2008**, *41*, 569.

(15) Zhao, Y.; Truhlar, D. G. *Acc. Chem. Res.* **2008**, *41*, 157.

(16) Zhao, Y.; Truhlar, D. G. *Theor. Chem. Acc.* **2008**, *120*, 215.

(17) Plumley, J. A.; Evanseck, J. D. *J. Chem. Theor. Comput.* **2008**, *4*, 1249.

(18) van Mourik, T. *J. Chem. Theor. Comput.* **2008**, *4*, 1610.

(19) Peverati, R.; Baldridge, K. K. *J. Chem. Theor. Comput.* **2008**, *4*, 2030.

(20) Sanford, M. S.; Love, J. A.; Grubbs, R. H. *J. Am. Chem. Soc.* **2001**, *123*, 6543.

(21) Tsipis, A. C.; Orpen, A. G.; Harvey, J. N. *Dalton Trans.* **2005**, 2849.

(22) Zhao, Y.; Truhlar, D. G. *Org. Lett.* **2007**, *9*, 1967.

(23) Parshall, G. W.; Ittel, S. D. *Homogeneus Catalysis*, 2nd ed.; Wiley: New York, 1992.

(24) *Handbook of Metathesis*; Grubbs, R. H., Ed.; Wiley-VCH: Weinheim, 2003.

(25) Pierotti, R. A. *Chem. Rev.* **1976**, *76*, 717.

(26) Tomasi, J.; Persico, M. *Chem. Rev.* **1994**, *94*, 2027.

(27) Tomasi, J.; Mennucci, B.; Cammi, R. *Chem. Rev.* **2005**, *105*, 2999.

(28) Jenn-Huei, L.; Allinger, N. L. *J. Comput. Chem.* **1998**, *19*, 1001. Lii, J. H.; Allinger, N. L. *J. Phys. Org. Chem.* **1994**, *7*, 591. Allinger, N. L.; Li, F. B.; Yan, L. Q. *J. Comput. Chem.* **1990**, *11*, 848. Allinger, N. L.; Li, F. B.; Yan, L. Q.; Tai, J. C. *J. Comput. Chem.* **1990**, *11*, 868. Allinger, N. L.; Geise, H. J.; Pyckhout, W.; Paquette, L. A.; Gallucci, J. C. *J. Am. Chem. Soc.* **1989**, *111*, 1106. Allinger, N. L.; Yuh, Y. H.; Lii, J. H. *J. Am. Chem. Soc.* **1989**, *111*, 8551. Lii, J. H.; Allinger, N. L. *J. Am. Chem. Soc.* **1989**, *111*, 8566. Lii, J. H.; Allinger, N. L. *J. Am. Chem. Soc.* **1989**, *111*, 8576.

(29) Ponder, J. W. *TINKER: Software Tools for Molecular Design; version 4.2.* Saint Louis, MO, 2004.

(30) Sipachev, V. A. *J. Mol. Struct.-THEOCHEM* **1985**, *22*, 143. Sipachev, V. A. In *Advances in Molecular Structure Research*; Hargittai, M., Hargittai, I., Eds.; JAI Press: Stamford, 1999; Vol. 5, pp 323−371.

(31) Becke, A. D. *J. Chem. Phys.* **1993**, *98*, 5648.

(32) Frisch, M. J.; Trucks, G. W.; Schlegel, H. B.; Scuseria, G. E.; Robb, M. A.; Cheeseman, J. R.; J. A, Montgomery, J.; Vreven, T.; Kudin, K. N.; Burant, J. C.; Millam, J. M.; Iyengar, S. S.; Tomasi, J.; Barone, V.; Mennucci, B.; Cossi, M.; Scalmani, G.; Rega, N.; Petersson, G. A.; Nakatsuji, H.; Hada, M.; Ehara, M.; Toyota, K.; Fukuda, R.; Hasegawa, J.; Ishida, M.; Nakajima, T.; Honda, Y.; Kitao, O.; Nakai, H.; Klene, M.; Li, X.; Knox, J. E.; Hratchian, H. P.; Cross, J. B.; Adamo, C.; Jaramillo, J.; Gomperts, R.; Stratmann, R. E.; Yazyev, O.; Austin, A. J.; Cammi, R.; Pomelli, C.; Ochterski, J. W.; Ayala, P. Y.; Morokuma, K.; Voth, G. A.; Salvador, P.; Dannenberg, J. J.; Zakrzewski, V. G.; Dapprich, S.; Daniels, A. D.; Strain, M. C.; Farkas, O.; Malick, D. K.; Rabuck, A. D.; Raghavachari, K.; Foresman, J. B.; Ortiz, J. V.; Cui, Q.; Baboul, A. G.; Clifford, S.; Cioslowski, J.; Stefanov, B. B.; Liu, G.; Liashenko, A.; Piskorz, P.; Komaromi, I.; Martin, R. L.; Fox, D. J.; Keith, T.; Al-Laham, M. A.; Peng, C. Y.; Nanayakkara, A.; Challacombe, M.; Gill, P. M. W.; Johnson, B.; Chen, W.; Wong, M. W.; Gonzalez, C.; Pople, J. A. *Gaussian 03; revision B.04*; Gaussian, Inc.: Pittsburgh, PA, 2003.

(33) Seeger, R.; Pople, J. A. *J. Chem. Phys.* **1977**, *66*, 3045. Bauernschmitt, R.; Ahlrichs, R. *J. Chem. Phys.* **1996**, *104*, 9047.

(34) Bergner, A.; Dolg, M.; Kuchle, W.; Stoll, H.; Preuss, H. *Mol. Phys.* **1993**, *80*, 1431.

(35) Feller, D. *J. Comput. Chem.* **1996**, *17*, 1571. Schuchardt, K. L.; Didier, B. T.; Elsethagen, T.; Sun, L. S.; Gurumoorthi, V.; Chase, J.; Li, J.; Windus, T. L. *J. Chem. Inf. Model.* **2007**, *47*, 1045.

(36) Dolg, M.; Wedig, U.; Stoll, H.; Preuss, H. *J. Chem. Phys.* **1987**, *86*, 866. Andrae, D.; Haussermann, U.; Dolg, M.; Stoll, H.; Preuss, H. *Theor. Chim. Acta* **1990**, *77*, 123.

(37) Dunning, T. H, Jr.; Hay, P. J. In *Methods of Electronic Structure Theory*; Schaefer, H. F.,III, Ed.; Plenum Press: New York, 1977, pp 1−27.

(38) Becke, A. D. *Phys. Rev. A* **1988**, *38*, 3098.

(39) Lee, C.; Yang, W.; Parr, R. G. *Phys. Rev. B* **1988**, *37*, 785. Miehlich, B.; Savin, A.; Stoll, H.; Preuss, H. *Chem. Phys. Lett.* **1989**, *157*, 200.

(40) Perdew, J. P.; Burke, K.; Ernzerhof, M. *Phys. Rev. Lett.* **1996**, *77*, 3865. Perdew, J. P.; Burke, K.; Ernzerhof, M. *Phys. Rev. Lett.* **1997**, *78*, 1396.

(41) Perdew, J. P.; W, Y. *Phys. Rev. B* **1986**, *33*, 8800.

(42) Becke, A. D. *J. Chem. Phys.* **1997**, *107*, 8554. Schmider, H. L.; Becke, A. D. *J. Chem. Phys.* **1998**, *108*, 9624.

(43) Bylaska, E. J.; Jong, W. A. d.; Govind, N.; Kowalski, K.; Straatsma, T. P.; Valiev, M.; Wang, D.; Apra, E.; Windus, T. L.; Hammond, J.; Nichols, P.; Hirata, S.; Hackler, M. T.; Zhao, Y.; Fan, P.-D.; Harrison, R. J.; Dupuis, M.; Smith, D. M. A.; Nieplocha, J.; Tipparaju, V.; Krishnan, M.; Wu, Q.; Voorhis, T. V.; Auer, A. A.; Nooijen, M.; Brown, E.; Cisneros, G.; Fann, G. I.; Fruchtl, H.; Garza, J.; Hirao, K.; Kendall, R.; Nichols, J. A.; Tsemekhman, K.; Wolinski, K.; Anchell, J.; Bernholdt, D.; Borowski, P.; Clark, T.; Clerc, D.; Dachsel, H.; Deegan, M.; Dyall, K.; Elwood, D.; Glendening, E.; Gutowski, M.; Hess, A.; Jaffe, J.; Johnson, B.; Ju, J.; Kobayashi, R.; Kutteh, R.; Lin, Z.; Littlefield, R.; Long, X.; Meng, B.; Nakajima, T.; Niu, S.; Pollack, L.; Rosing, M.; Sandrone, G.; Stave, M.; Taylor, H.; Thomas, G.; Lenthe, J. v.; Wong, A.; Zhang, Z. *NWChem, A Computational Chemistry Package for Parallel Computers; 5.1*; Pacific Northwest National Laboratory: Richland, WA, 2007.

(44) Martin, J. M. L.; Sundermann, A. *J. Chem. Phys.* **2001**, *114*, 3408.

(45) Møller, C.; Plesset, M. S. *Phys. Rev.* **1934**, *46*, 618.

(46) Boys, S. F.; Bernardi, F. *Mol. Phys.* **1970**, *19*, 553.

(47) Woon, D. E.; Dunning, T. H. *J. Chem. Phys.* **1993**, *98*, 1358.

(48) Dunning, T. H. *J. Chem. Phys.* **1989**, *90*, 1007.

(49) Cossi, M.; Scalmani, G.; Rega, N.; Barone, V. *J. Chem. Phys.* **2002**, *117*, 43.

(50) Tomasi, J. *Theor. Chem. Acc.* **2004**, *112*, 184.

(51) Cramer, C. J.; Truhlar, D. G. *Acc. Chem. Res.* **2009**, *42*, 493.

(52) Klamt, A.; Mennucci, B.; Tomasi, J.; Barone, V.; Curutchet, C.; Orozco, M.; Luque, F. J. *Acc. Chem. Res.* **2009**, *42*, 489.

(53) Cramer, C. J.; Truhlar, D. G. *Acc. Chem. Res.* **2008**, *41*, 760.

(54) Klamt, A.; Schuurmann, G. *J. Chem. Soc., Perkin Trans. 2* **1993**, 799.

(55) Tannor, D. J.; Marten, B.; Murphy, R.; Friesner, R. A.; Sitkoff, D.; Nicholls, A.; Ringnalda, M.; Goddard, W. A.; Honig, B. *J. Am. Chem. Soc.* **1994**, *116*, 11875.

(56) Pais, A.; Sousa, A.; Eusebio, M. E.; Redinha, J. S. *Phys. Chem. Chem. Phys.* **2001**, *3*, 4001.

(57) Amovilli, C.; Mennucci, B. *J. Phys. Chem. B* **1997**, *101*, 1051.

(58) Claverie, P. In *Intermolecular Interactions: From Diatomics to Biopolymers*; Pullman, B., Ed.; Wiley: New York, 1978; Vol. 1, p 69.

(59) Bidon-Chanal, A.; Huertas, O.; Orozco, M.; Luque, F. J. *Theor. Chem. Acc.* **2009**, *123*, 11.

(60) Mintz, C.; Ladlie, T.; Burton, K.; Clark, M.; Acree, W. E.; Abraham, M. H. *QSAR Comb. Sci.* **2008**, *27*, 627.

(61) Nguyen, S. T.; Johnson, L. K.; Grubbs, R. H.; Ziller, J. W. *J. Am. Chem. Soc.* **1992**, *114*, 3974. Schwab, P.; France, M. B.; Ziller, J. W.; Grubbs, R. H. *Angew. Chem., Int. Ed. Engl.* **1995**, *34*, 2039. Trnka, T. M.; Grubbs, R. H. *Acc. Chem. Res.* **2001**, *34*, 18.

(62) Vyboishchikov, S. E.; Bühl, M.; Thiel, W. *Chem.—Eur. J.* **2002**, *8*, 3962.

(63) Torker, S.; Merki, D.; Chen, P. *J. Am. Chem. Soc.* **2008**, *130*, 4808.

(64) Sanford, M. S.; Ulman, M.; Grubbs, R. H. *J. Am. Chem. Soc.* **2001**, *123*, 749.

(65) Straub, B. F. *Adv. Synth. Catal.* **2007**, *349*, 204.

(66) Cavallo, L. *J. Am. Chem. Soc.* **2002**, *124*, 8965.

(67) *Jaguar; version 4.0*; Schrödinger Inc.: Portland, OR, 2000.

(68) Harvey, J. N. Personal communication.

(69) Darensbourg, D. J.; Graves, A. H. *Inorg. Chem.* **1979**, *18*, 1257.

(70) Wovkulich, M. J.; Feinberg, S. J.; Atwood, J. D. *Inorg. Chem.* **1980**, *19*, 2608.

(71) Wovkulich, M. J.; Atwood, J. D. *Organometallics* **1982**, *1*, 1316.

(72) Lichtenberger, D. L.; Brown, T. L. *J. Am. Chem. Soc.* **1978**, *100*, 366.

(73) Rigo, P.; Guastall., G; Turco, A. *Inorg. Chem.* **1969**, *8*, 375.

(74) Rigo, P.; Pecile, C.; Turco, A. *Inorg. Chem.* **1967**, *6*, 1636.

JP902940C